Exclusion process on two intersecting lanes with constrained resources: Symmetry breaking and shock dynamics

Akriti Jindal and Arvind Kumar Gupta*
Department of Mathematics, Indian Institute of Technology Ropar, Rupnagar 140001, Punjab, India

(Received 3 November 2020; revised 14 May 2021; accepted 9 July 2021; published 27 July 2021)

We present a study of the exclusion process on a peculiar topology of network with two intersecting lanes, competing for the particles in a reservoir with finite capacity. To provide a theoretical ground for our findings, we exploit mean-field approximation along with domain-wall theory. The stationary properties of the system, including phase transitions, density profiles, and position of the domain wall are derived analytically. Under the similar dynamical rules, the particles of both lanes interact only at the intersected site. The symmetry of the system is maintained until the number of particles do not exceed the total number of sites. However, beyond this, the symmetry breaking phenomenon occurs, resulting in the appearance of asymmetric phases and continues to persist even for an infinite number of particles. The complexity of the phase diagram shows a nonmonotonic behavior with an increasing number of particles in the system. A bulk induced shock appears in a symmetric phase, whereas, a boundary induced shock is observed in the symmetric as well as the asymmetric phase. Monitoring the location of localized shock with increasing entry of particles, we explain the possible phase transitions. The theoretical results are supported by extensive Monte Carlo simulations and explained using simple physical arguments.

DOI: 10.1103/PhysRevE.104.014138

I. INTRODUCTION

The decisive requirement for the functioning of any complex system ranging from the subcellular level of biological organisms to globe-spanning human-made structures is the transportation of matter and information. From a theoretical point of view, these stochastic transport phenomena are an intriguing example of multiparticle systems addressing far from equilibrium processes. The extensive organization of interconnected linelike pathways for transport mechanisms forms a networklike structure. However, the study of complex frameworks remains a major challenge in the field of physics and cellular biology. In this direction, the investigation of relatively simpler topologies is crucial for understanding the complex network systems.

In statistical physics, lattice gas exclusion processes have gained much popularity to model the active stochastic motion of particles along a one-dimensional lane [1–3]. Specifically, the totally asymmetric simple exclusion process (TASEP) has been a paradigmatic model to study the motion of self-propelled particles in one preferred direction subjected to excluded volume interactions [4,5]. It was originally introduced in the context of RNA polymerization by ribosomes [1,6,7]. Since then, these models have further stimulated a lot of fundamental research, including vehicular traffic, intracellular transport, surface growth, transport in ion channels, etc. [6,8–11]. In terms of the TASEP, numerous simpler topologies, such as junctions, treelike structures, and structureless links have been extensively analyzed in traffic flow and biological transportation [12–15]. However, particles' collective behavior on elementary structures of networks is still a subject of comprehensive discussion.

In the perspective of modeling generic features of transportation processes on lane-based systems, studies abound in the literature analyzing the topology of intersecting lanes, crossing pedestrian traffic flows [16–20]. Furthermore, recently the generic cytoskeletal transport features of motor proteins passing through three-dimensional (3D) filament crossings have been explored [21]. The 3D structure of the crossing is unwrapped into an ensemble of one-dimensional (1D) or quasi-1D paths with branching points located at the crossing where motor proteins can either follow the same lane or change their paths. The collective dynamics of motor proteins is strongly influenced by the steric hinderance induced due to interaction of moving entities at the crossings. Owing to an extensive body of the TASEP models, quantitative characterization of two crossing roads with parallel update rules in a closed geometry has been well examined [22–25]. Recently, a variant of the TASEP network considering "figure-of-eight" topology of two intersecting lanes has been studied where particles move in accordance to random sequential update rules [26]. This prototype provides an insight into the Braess paradox that explains the counterintuitive situation. Adding an edge to a road network leads to a user optimum with higher travel times for all network users [27,28]. However, the dynamics of two intersecting lanes with open boundary conditions revealed a much interesting phenomenon known as spontaneous symmetry breaking (SSB) [25,29–31]. This displays the occurrence of macroscopic asymmetric stationary states under the symmetric microscopic dynamical rules. The"bridge model" was the pioneer model to exhibit SSB

*akgupta@iitrpr.ac.in

where two species of particles are allowed to move in the opposite direction on a single lane TASEP [32,33]. Since then this aspect has been of specific interest studied in detail utilizing variants of the TASEP assimilating various additional processes [34–38]. Such models have been thoroughly investigated in the vicinity of an unlimited supply of particles. However, it is still a challenge to completely uncover various features of biological and physical models of intersecting lanes based on generic dynamical rules.

In recent years, much more generalized versions of the TASEP model have been contemplated where the particles are injected from a finite reservoir of particles. Such models have shown wide applicability in many physical and biological systems, such as protein synthesis, movement of motor proteins, "parking garage problems," and vehicular traffic [39–41]. For example, *invitro* experiments performed at motor protein concentrations that are low with respect to the concentrations of polymerized tubulin heterodimers can lead to the limited available resources [42]. Moreover, during protein synthesis, the ribosomes disassemble from messenger RNA after the translation process. Under rapid cell growth, the ribosomes find themselves in short supply so that a self-limitation of translation can occur. To explore such a scenario originating due to real-time dynamics invoked by limited resources studies based on single as well as multilane TASEP prototypes have been conducted [39,43–46]. This generalization reveals a nontrivial behavior of system including the extension of "shock phase" that leads to traffic jamlike situations on lanes. For this phase domain-wall approach provides a powerful theoretical technique to incorporate fluctuations and accurately calculate the stationary properties of the system [46].

Although biological and vehicular traffic is our basic motivation, we present below a model which has an intrinsic interest that extends beyond this particular application. From a wider perspective, the proposed model presents a minimalistic analysis of driven nonequilibrium transport process through intersecting lanes by considering the limited availability of resources. Our results allow us to address analytically how this competition of finite resources on intersecting pathways influences the density profile and leads to a jam situation on filaments. We treat this model as a two-lane coupled system with an inhomogeneity for which we exploit the idea of effective rates and domain-wall theory to analyze the interplay of the intersected site and finite reservoir. In particular, we derive explicit expressions of density profiles, determine the parameter range for which we expect jam formation and symmetry breaking. Additionally, our purpose is to inspect whether the symmetry breaking phenomenon prevails in the system with finite number of particles. And, if it persists can it be controlled by a varying number of particles.

We also provide a fundamental brief by considering appropriate limiting cases to visualize the steady-state characteristics of the system.

II. MODEL DEFINITION AND DYNAMICAL RULES

This section intends to elaborate a minimalistic model of two-lane transport intersecting at a special site. The extreme ends of both lanes are coupled to a single reservoir having a finite number of identical particles denoted by N_r. The total number of particles (N_{tot}) in the system remains constant at any instant of time. The two lanes are labeled L and T assuming each lane to be composed of $i = 1, 2, \ldots, N$ sites with a special site at $k = N/2$ common to both the lanes as shown in Fig. 1. We assume this site far away from boundaries to probe the effect of intersecting lanes on the overall dynamics of the system. A lane is randomly chosen, and the transition rules are implemented in accordance to random sequential update rules. Each site including the intersected site obeys the hard core exclusion principle that allows each site to occupy at most one particle.

We presume particles in both lanes to move in one preferred direction from left to right. A particle is allowed to enter the first vacant site of any of the two lanes from the reservoir with effective intrinsic rate α^* depending on the reservoir density given by

$$\alpha^* = \alpha f(N_r), \tag{1}$$

where α is the entry rate for the case with an infinite number of particles.

It is reasonable to adopt a monotonic increasing function satisfying $f(0) = 0$ and $f(N_{\text{tot}}) = 1$. This means the smaller the number of particles in the reservoir, the lower the effective intrinsic rate of particles in the two lanes. And, the enhanced particle content in the reservoir leads to greater rush of particles in the two lanes. Based on these arguments, the simplified choice for $f(N_r)$ is as follows:

$$f(N_r) = \frac{N_r}{N_{\text{tot}}}, \tag{2}$$

that implies the effective intrinsic rate given by [44]

$$\alpha^* = \alpha \frac{N_r}{N_{\text{tot}}}. \tag{3}$$

This relation implies that the entry rate of particles is directly proportional to the free concentration of particles in the reservoir as long as it is not too crowded. The choice of function is generic and suits well to imitate biological as well as vehicular transport processes [39–41]. For either lane, the exit rate of particles is independent of the number of particles present in the reservoir. A particle at site N can escape with constant rate β back to the reservoir from where it is free to rejoin any lane.

In the bulk of each lane, a particle seeks to jump to the adjacent vacant site of the same lane with the unit rate and are not allowed to switch their lanes. However, the intersection of two lanes at site k distinguishes it from a homogeneous two-lane TASEP model [16,30]. Since site k is shared by both lanes, any of the particle approaching from lane L or T can occupy this site at any instant of time. A particle at site $k-1$ of lane $L(T)$ can jump to intersected site k with the unit rate if found empty. Furthermore, if site k is occupied with the particle arriving from lane L or T, it is allowed to jump to the unoccupied site $k+1$ of its own respective lane with rate 1. Here, the particles are not allowed to change their lanes even after jumping from the intersected site. For the proposed model, particles of both lanes interact only at the intersected site because a particle at site $k-1$ of lane $L(T)$ compete to find an empty site k.

It has been noted that for the case of the infinite number of particles, the considered topology of lanes induces a nontrivial

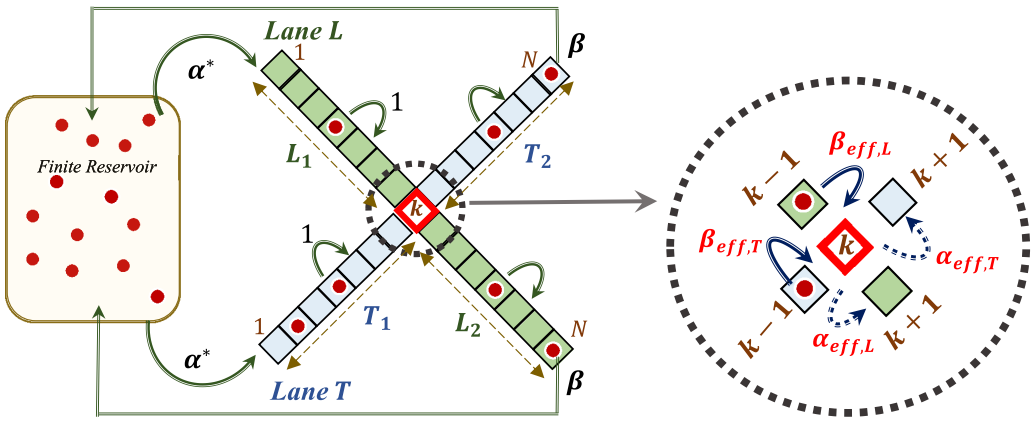

FIG. 1. Schematic representation of two intersecting lanes in a reservoir with a finite number of particles. Green and blue colored lanes represent lanes L and T, respectively, with $i = 1, 2, \ldots, N$ labeled sites. The intersected site $k = N/2$ is highlighted in the red color that can occupy any of the particle arriving from lane L or T. If this site accommodates a particle from $L(T)$ it can jump to the unoccupied site $k+1$ of same lane with the unit rate. The particles are allowed to enter any of the two lanes with effective intrinsic rate α^* given by Eq. (3) and escape the lane with rate β. Each lane $L(T)$ is divided into two parts of a left segment $L_1(T_1)$ and a right segment $L_2(T_2)$. The particles can leave $L_1(T_1)$ with effective exit rate $\beta_{\mathrm{eff},L}(\beta_{\mathrm{eff},T})$ and enter into $L_2(T_2)$ with the effective entry rate $\alpha_{\mathrm{eff},L}(\alpha_{\mathrm{eff},T})$.

effect on the qualitative behavior of the system in terms of symmetry breaking [30]. However, in the previous work, the existence of phase regimes specially for an asymmetric phase is calculated numerically.

III. THEORETICAL FRAMEWORK

The present model can be viewed as a variant of the TASEP model with two incoming segments reaching a junction site and diverging into two outgoing segments [13]. This represents a network of 2×2 segments provided the particles at site k are distinguishable and are constrained to jump to the next site of specific lane. To begin with the theoretical framework of our proposed model, we first briefly recall the results of the two-lane parallel uncoupled homogeneous TASEP model with an infinite number of particles in the system.

A. Brief discussion of results for the two-lane homogeneous TASEP model with an infinite reservoir

In literature, mean-field approximation has been discerned to predict exact phase boundaries for the homogeneous single-lane TASEP model with an infinite reservoir where particles move in accordance to random sequential update rules [11,47–50]. It has been found that there exists three distinct stationary phases: low density (LD), high density (HD), and maximal current (MC) [11,47–50]. Various network TASEP models have been extensively explored utilizing mean-field theory [12–15,28,51]. This approximation ignores all possible correlations in the system and assumes the occupancy of two consecutive sites independent of each other.

Based on this approach, it can be trivially deliberated that for equal entry and exit rates of two uncoupled lanes (L and T), there exist three dynamic regimes, namely, LD:LD, HD:HD, and MC:MC. The bulk density in each phase remains equal for both lanes, leading to the existence of symmetric phases. In the notation, the first part of : denotes the state of lane L, and second part describes the phase manifested by lane T. The description of theoretically calculated density profiles, particle currents, and existence of phases is summarized in Table I. The average density of particles at site i in two lanes L and T is represented by ρ^i and σ^i, respectively. In thermodynamic limit $N \gg 1$, the steady-state average density of particles is a function of the spatial variable written as $\rho(x) \equiv \rho^i$, where $x = i/N$ ranging from [0,1]. Following mean-field approximation the steady-state particle current in the bulk ($1 < i < N$) of lanes L and T is denoted by J_L and J_T, respectively, given by

$$J_L = \rho(x)[1-\rho(x)], \qquad J_T = \sigma(x)[1-\sigma(x)]. \tag{4}$$

Since the current is constant throughout the lane, the script (x) in each lane can be dropped to avoid repetition throughout the paper. Similarly, the current at sites 1 and N of each lane can be written as

$$J_L^1 = \alpha(1-\rho^1), \qquad J_L^N = \rho^N\beta, \tag{5}$$

$$J_T^1 = \alpha(1-\sigma^1), \qquad J_T^N = \sigma^N\beta, \tag{6}$$

where $\rho^1(\sigma^1)$ and $\rho^N(\sigma^N)$ represent the average density of particles at sites 1 and N, respectively, of lane $L(T)$.

B. Bulk dynamics: Intersection of two lanes

The intersection of two lanes at a special site introduces an inhomogeneity in the system. For this, we divide each lane into two segments, the left segment L_1, T_1: $i = 1, 2, \ldots, k-1$ and the right segment L_2, T_2: $i = k+1, k+2, \ldots, N$ coupled at special site k. The two segments of both lanes are properly integrated by determining the effective rate of particles. We define, particles entering in lanes L and T with effective intrinsic rate α^* [defined in Eq. (3)] can leave their respective left segment with effective exit rates $\beta_{\mathrm{eff},L}$ and $\beta_{\mathrm{eff},T}$, respectively. And the particles can enter the right segment of lanes L and T with effective entry rates $\alpha_{\mathrm{eff},L}$ and $\alpha_{\mathrm{eff},T}$, respectively. The average density of particles at site

TABLE I. Summary of results for a two uncoupled lane TASEP model with a finite reservoir where $\mu = \frac{N_{\rm tot}}{N}$ [44]. When $\mu \to \infty$, $\alpha^* \to \alpha$, the results converge to that for the model with an infinite reservoir of particles [4]. Here, LD signifies the low-density phase, HD denotes the high-density phase, and x_w denotes the position of the domain wall in the Shock (S) phase. The expression of the S:S phase is valid only for the case when μ is finite.

	Phase region	$\rho^1 = \sigma^1$	$\rho = \sigma$	$\rho^N = \sigma^N$	Current ($J_L = J_T$)	α^*
LD:LD	$\alpha^* < \min\{\beta, 1/2\}$	α^*	α^*	$\frac{\alpha^*(1-\alpha^*)}{\beta}$	$\alpha^*(1-\alpha^*)$	$\alpha\left(1-\frac{1}{\mu}\right)$
HD:HD	$\beta < \min\{\alpha^*, 1/2\}$	$1-\frac{\beta(1-\beta)}{\alpha^*}$	$1-\beta$	$1-\beta$	$\beta(1-\beta)$	$\alpha\left(1-\frac{2(1-\beta)}{\mu}\right)$
MC:MC	$1/2 < \min\{\alpha^*, \beta\}$	$1-\frac{1}{4\alpha^*}$	$\frac{1}{2}$	$\frac{1}{4\beta}$	$\frac{1}{4}$	$\alpha\left(1-\frac{1}{\mu}\right)$
S:S	$\alpha^* = \beta,\ \beta < 1/2$	α^*	$x_w\alpha^* + (1-\beta)(1-x_w)$	$1-\beta$	$\alpha^*(1-\alpha^*) = \beta(1-\beta)$	$\frac{1}{x_w}\left[\frac{\mu}{2\alpha}(\alpha-\beta) - (1-\beta)(1-x_w)\right]$

$k-1$, k and $k+1$ of lane L is written as ρ_1^{k-1}, ρ^k, and ρ_2^{k+1}. Similarly, for lane T to represent these densities ρ is replaced by σ.

We denote the particle current induced in each lane as J_{L_j} and J_{T_j} where $j = 1$ (left segment) and $j = 2$ (right segment). The stationary current arguments in both lanes leads to an equal current in two segments of each lane read as

$$J_{L_1} = J_{L_2} \quad \text{and} \quad J_{T_1} = J_{T_2}, \tag{7}$$

that implies

$$\rho_1^b(1-\rho_1^b) = \rho_2^b(1-\rho_2^b) \text{ and } \sigma_1^b(1-\sigma_1^b) = \sigma_2^b(1-\sigma_2^b), \tag{8}$$

where ρ_j^b and σ_j^b denote the bulk density in two segments of lanes L and T, respectively. The above equations in Eq. (8) further specifies that the bulk density satisfies

$$\rho_1^b = \rho_2^b \quad \text{or} \quad \rho_1^b + \rho_2^b = 1, \tag{9}$$

$$\sigma_1^b = \sigma_2^b \quad \text{or} \quad \sigma_1^b + \sigma_2^b = 1. \tag{10}$$

In each lane, the condition of current continuity suggests that the exit current of the left segment is equal to the current passing from site $k-1$ to k, given by

$$\rho_1^{k-1}\beta_{\text{eff},L} = \rho_1^{k-1}(1-\rho^k-\sigma^k), \tag{11}$$

$$\sigma_1^{k-1}\beta_{\text{eff},T} = \sigma_1^{k-1}\,(1-\rho^k-\sigma^k), \tag{12}$$

that results in

$$\beta_{\text{eff},L} = \beta_{\text{eff},T} = 1-\rho^k-\sigma^k = \beta_{\text{eff}} \text{ (say)}. \tag{13}$$

Also, the current entering into the right segment is equal to current passing from site k to $k+1$, written as

$$\left(1-\rho_2^{k+1}\right)\alpha_{\text{eff},L} = \rho^k\left(1-\rho_2^{k+1}\right), \tag{14}$$

$$\left(1-\sigma_2^{k+1}\right)\alpha_{\text{eff},T} = \sigma^k\,\left(1-\sigma_2^{k+1}\right), \tag{15}$$

that leads to

$$\alpha_{\text{eff},L} = \rho^k, \tag{16}$$

$$\alpha_{\text{eff},T} = \sigma^k. \tag{17}$$

Our main aim is to calculate the effective rates and average density of particles in L and T including at the intersected site. The explicitly computed effective rates helps to determine the stationary properties of the system. When there are infinite numbers of particles in the system, it has been observed that the intersection of lanes assists the phenomenon of symmetry breaking. The appearance of two symmetric and one asymmetric phase has been reported [30].

C. Boundary dynamics: Lanes connected to the finite reservoir of particles

The extreme ends of two intersecting lanes are coupled to a finite reservoir of particles that governs the effective intrinsic rate of particles into the lanes as given in Eq. (3). Now, the total number of particles in the system can be written as

$$N_{\rm tot} = N_r + N_L + N_T, \tag{18}$$

where N_L and N_T signify the number of particles in lanes L and T, respectively.

Since each lane is divided in two segments, the average density of particles in each lane is the sum of average density of particles in the respective left and right segment. Therefore, in continuum limit we can write the average density of particles integrating over x in lanes L and T as

$$\int_0^1 \rho(x)dx = \int_0^{1/2} \rho_1^b(x)dx + \int_{1/2}^1 \rho_2^b(x)dx, \tag{19}$$

$$\int_0^1 \sigma(x)dx = \int_0^{1/2} \sigma_1^b(x)dx + \int_{1/2}^1 \sigma_2^b(x)dx, \tag{20}$$

respectively, where $\int_0^1 \rho(x)dx = \frac{N_L}{N}$ and $\int_0^1 \sigma(x)dx = \frac{N_T}{N}$. Furthermore, the effective intrinsic rate in Eq. (3) can be written as

$$\alpha^* = \alpha - \frac{\alpha N}{N_{\rm tot}}\left(\int_0^{1/2}\left(\rho_1^b+\sigma_1^b\right)dx + \int_{1/2}^1\left(\rho_2^b+\sigma_2^b\right)dx\right), \tag{21}$$

that implies

$$\alpha^* = \alpha - \frac{\alpha}{\mu}\left(\int_0^{1/2}\left(\rho_1^b+\sigma_1^b\right)dx + \int_{1/2}^1\left(\rho_2^b+\sigma_2^b\right)dx\right), \tag{22}$$

where

$$\mu = \frac{N_{\rm tot}}{N}. \tag{23}$$

As already observed in Table I that the density of particles is distinct in each phase, therefore, the effective intrinsic rate

α^* alters correspondingly. For the case when two lanes do not intersect, we retrieve a two-lane homogeneous model coupled to a finite reservoir of particles. Therefore, the expression for effective intrinsic rate in Eq. (22) reduces to [43]

$$\alpha^* = \alpha\left(1 - \frac{1}{\mu}\int_0^1 (\rho + \sigma)dx\right). \tag{24}$$

Here, in addition to existing distinct stationary phases for the homogeneous two-lane model with an infinite reservoir, a new symmetric coexistence LD-HD phase, namely, the S phase has been observed [44]. A localized shock phase is characterized by an existing discontinuity in the bulk connected by a low-density to high-density regime. In literature, a well-known approach " domain-wall theory" has been deployed to estimate the position of the localized domain wall [43,50,52]. The basic idea of this theory is to assume a sharp shock in the density profile located at any site between the two regimes: LD to the left and HD to the right of the domain wall. The estimation of locating this localized shock at a particular site helps to evaluate the overall density of particles. This shock is situated anywhere between [0,1], and its position is denoted by x_w throughout the paper. The conditions for the existence of stationary phases with finite reservoirs have been reviewed in Table I.

In the next section, we discuss the conditions for the existence of different phase regimes on the (α, β) plane for the proposed inhomogeneous model of intersecting lanes. The phase boundaries are obtained theoretically utilizing the framework adopted in Sec. III B along with the concept of domain-wall theory. In addition, we present the convergence of our theoretical results to the limiting case of intersecting lanes with infinite reservoirs [30].

IV. STATIONARY SYSTEM STATES

In this section we elaborate the qualitative and quantitative behaviors of stationary phase diagrams depending on three controlling parameters (α, β, μ). As already discussed, each lane L (T) is divided into two segments L_1 and L_2 (T_1 and T_2), the possible phases in the system are labeled as *A*-*B*:*C*-*D* where A (C) and B (D) describe the phase exhibited by left and right segments of lane L (T), respectively. In addition, a phase is characterized as a symmetric phase if the particle density in $L_1(L_2)$ is equal to density in $T_1(T_2)$ (i.e., $\rho_1^b = \sigma_1^b$ and $\rho_2^b = \sigma_2^b$). Otherwise, the phase is indicated as a asymmetric phase and is labeled in *italics*.

For the proposed model, each segment can exhibit four possible stationary states LD, HD, MC, or S. Therefore, the maximum possible number of stationary phases in each lane is $4^2 = 16$. However, the existence of an ample number of phases is prohibited due to various restrictions. For example, from Eq. (7) it can be easily realized that for either lane, the possibility of having the MC phase in any of the segments and the LD, HD, or S in the other segment can be discarded because these phases support different particle currents. Moreover, both segments cannot exhibit MC phase simultaneously. This is because if the left segment shows an average density $1/2$, the inhomogeneous dynamical rules do not allow the right segment to achieve maximal current. Also, due to interaction of particles at site k, the right segments of both lanes cannot exhibit the HD phase simultaneously since a particle at site k is restricted to jump only in the same lane. As a consequence, when any of particle arriving from lane L or T resides on the intersected site, the particle on site $k-1$ of the other lane has to wait until the particle at the kth site jumps to the site of its own respective lane. The similar arguments can affirm the existence of the asymmetric phase in the system of intersecting lanes with an infinite number of particles [30]. Nevertheless, the limiting case of the proposed model with an infinite number of particles will be extensively discussed.

Now we theoretically investigate the conditions of the existence of phases, phase boundaries for the proposed model with varying entry and exit rates. We provide explicit expressions for the density profiles, phase boundaries, and position of shock in terms of μ. Since for the proposed model both symmetric and asymmetric phases can exist, we systematically discuss the existence condition of symmetric and asymmetric phases in the upcoming sections.

A. Symmetric phases

We now discuss the occurrence of different symmetric phases and aim to calculate the effective rates and densities to determine the phase boundaries. As discussed, for the symmetric phase the following conditions hold, i.e.:

$$\rho_1^b = \sigma_1^b, \qquad \rho_2^b = \sigma_2^b, \tag{25}$$

that also implies

$$\alpha_{\text{eff},L} = \alpha_{\text{eff},T} = \alpha_{\text{eff}}, \qquad \rho^k = \sigma^k. \tag{26}$$

Without any loss of generality, we can, thus, analyze the dynamics of particles in any one lane (say L). The same results are pertinent for the other lane T. Hence, Eq. (22) reduces to

$$\alpha^* = \alpha - \frac{2\alpha}{\mu}\left(\int_0^{1/2} \rho_1^b dx + \int_{1/2}^1 \rho_2^b dx\right). \tag{27}$$

Therefore, by utilizing the current continuity condition we can explicitly compute effective rates α^*, α_{eff} and β_{eff} to determine theoretical phase boundaries, shock position, and particle densities in possible phases.

As a consequence, there are four possible symmetric phases, namely, LD-LD:LD-LD, HD-LD:HD-LD, S-LD:S-LD, LD-S:LD-S. We summarize the existence criteria, expressions of shock position and effective intrinsic rate for all symmetric phases in Table II. The detailed calculations of effective rates, densities, and phase boundaries in each possible symmetric phase are illustrated in Appendix A.

B. Asymmetric phases

Asymmetric phases appear along with the symmetric phases due to interaction of both type of particles at the intersected site. In contrast to symmetric phases, the density of particles in both lanes is different. Therefore, the specifications that support the extant of asymmetric phases can be written as

$$\rho_1^b \neq \sigma_1^b \quad \text{or} \quad \rho_2^b \neq \sigma_2^b, \tag{28}$$

that can lead to

$$\alpha_{\text{eff},L} \neq \alpha_{\text{eff},T}, \quad \rho^k \neq \sigma^k. \tag{29}$$

TABLE II. Explicit expressions for the conditions of existence, effective intrinsic rate, and shock position in the possible symmetric phases of the proposed model. The detailed calculations are derived in Appendix A.

Phase	Phase region	Intrinsic rate α^*	x_w
LD-LD:LD-LD	$\alpha^* < \min\{\beta, 1/3\}$	$\frac{\alpha\mu}{\mu+2\alpha}$	–
HD-LD:HD-LD	$1/3 < \min\{\alpha^*, \beta\}$	$\alpha\left(1-\frac{1}{\mu}\right)$	–
S-LD:S-LD	$0 < x_w < 1/2,\ \beta \geqslant 1/3$	$\alpha\left(\frac{3\mu+2x_w-4}{3\mu}\right)$	$\frac{3}{2}\left(\frac{\mu}{3\alpha}-\mu+1\right)$
LD-S:LD-S	$1/2 < x_w < 1,\ \beta \leqslant 1/3$	β	$\frac{\beta\mu-\alpha(\mu+2\beta-2)}{2\alpha(1-2\beta)}$

To theoretically derive the phase boundaries, position of shock and particle density in each lane for the possible asymmetric phases, we calculate effective rates by using current continuity arguments.

As a result, there are two possible asymmetric phases, namely, S-HD:HD-LD and HD-HD:HD-LD for which the existence criteria, expressions of shock position and effective intrinsic rate are summarized in Table III. The theoretical computations for the expressions of densities and phase boundaries are explained in Appendix B.

V. RESULTS AND DISCUSSIONS

In this section, we exploit the results discussed in Sec. IV to address the behavior of the system on the (α, β) plane depending on the total number of particles in the system. We aim to investigate the effect of finite resources in terms of $\mu = \frac{N_{\text{tot}}}{N}$ on the complex dynamical properties of the system. We observe qualitative as well as quantitative nontrivial effects on the topology of phase schema especially in terms of symmetry breaking and shock dynamics. To validate our theoretical outcomes we perform elementary Monte Carlo simulations (MCs) for system size $N = 1000$. Following the random sequential update rule, each simulation step generates one specific realization of the stochastic process. At each time step, a lane is randomly chosen and utilizing uniformly generated random number a particular site is selected on which the transition rules are implemented as discussed in Sec. II. The computer simulations are carried out for 2×10^9 time steps, and an initial 5% of the time steps are scraped to ensure the occurrence of the steady state. The average densities in both lanes are computed by considering time averages over an interval of $10N$. We observe that the theoretically computed density profiles, phase boundaries, and shock positions match well with the simulations.

A. Phase boundaries: Effect of μ

We have theoretically computed the existence of distinct stationary phases in terms of μ where we analyzed that the symmetry of the system persists for $\mu \leqslant 1$. However, for $\mu > 1$ the symmetry of the system is disrupted and asymmetric phases appear in the stationary phase diagram. To understand the effect of finite resources, we elaborate two different cases and possible phase transitions originating in the system by monitoring the propagation of the localized domain wall in the steady state for varying boundary controlling parameters.

1. $\mu \leqslant 1$

When there are very few numbers of particles in the system, i.e., $\mu \approx 0$, only one symmetric phase, namely, LD-LD:LD-LD appears in the entire phase regime as presented in Fig. 2(a) for $\mu = 0.001$. This can be easily realized by a simple argument that due to scarcity of particles in the reservoir fewer number of particles are allowed to enter any of the lanes, leading to the low-density phase in each segment. Also, for lower values of β the particles tend to accumulate at the right end of each lane. As a consequence, the boundary layer at the right boundary enters the bulk leading to the emergence of boundary induced shock in the right segment. Thus, a symmetric phase, namely, the LD-S:LD-S phase appears in the phase diagram for $\mu > 0$ as shown in Fig. 2(b) for $\mu = 0.05$. The phase boundary between these two phases is obtained from Eq. (A33) given by

$$\alpha = \frac{\beta\mu}{\mu - 2\beta}, \qquad \beta \leqslant 1/3. \tag{30}$$

With a significant increase in μ no qualitative changes are observed in the system except the shifting of phase boundaries resulting in the shrinkage of the LD-LD:LD-LD phase and expansion of the LD-S:LD-S phase. However, beyond a critical value μ_{C_1} due to interaction of particles at the intersected site

TABLE III. Explicit expressions for the conditions of existence, effective intrinsic rate, and shock position in the possible asymmetric phases of the proposed model. The detailed calculations are derived in Appendix B.

Phase	Phase region	Intrinsic rate α^*	x_w
S-HD:HD-LD	$0 < x_w < 1/2,\ \beta \leqslant 1/3$	β	$\frac{2\mu(\beta-\alpha)+\alpha(3-2\beta)}{2\alpha(1-2\beta)}$
HD-HD:HD-LD	$\frac{\alpha(3-2\mu)}{2(\alpha-\mu)} < \beta,\ \beta \leqslant 1/3$	$\alpha\left(\frac{2\mu+2\beta-3}{2\mu}\right)$	–

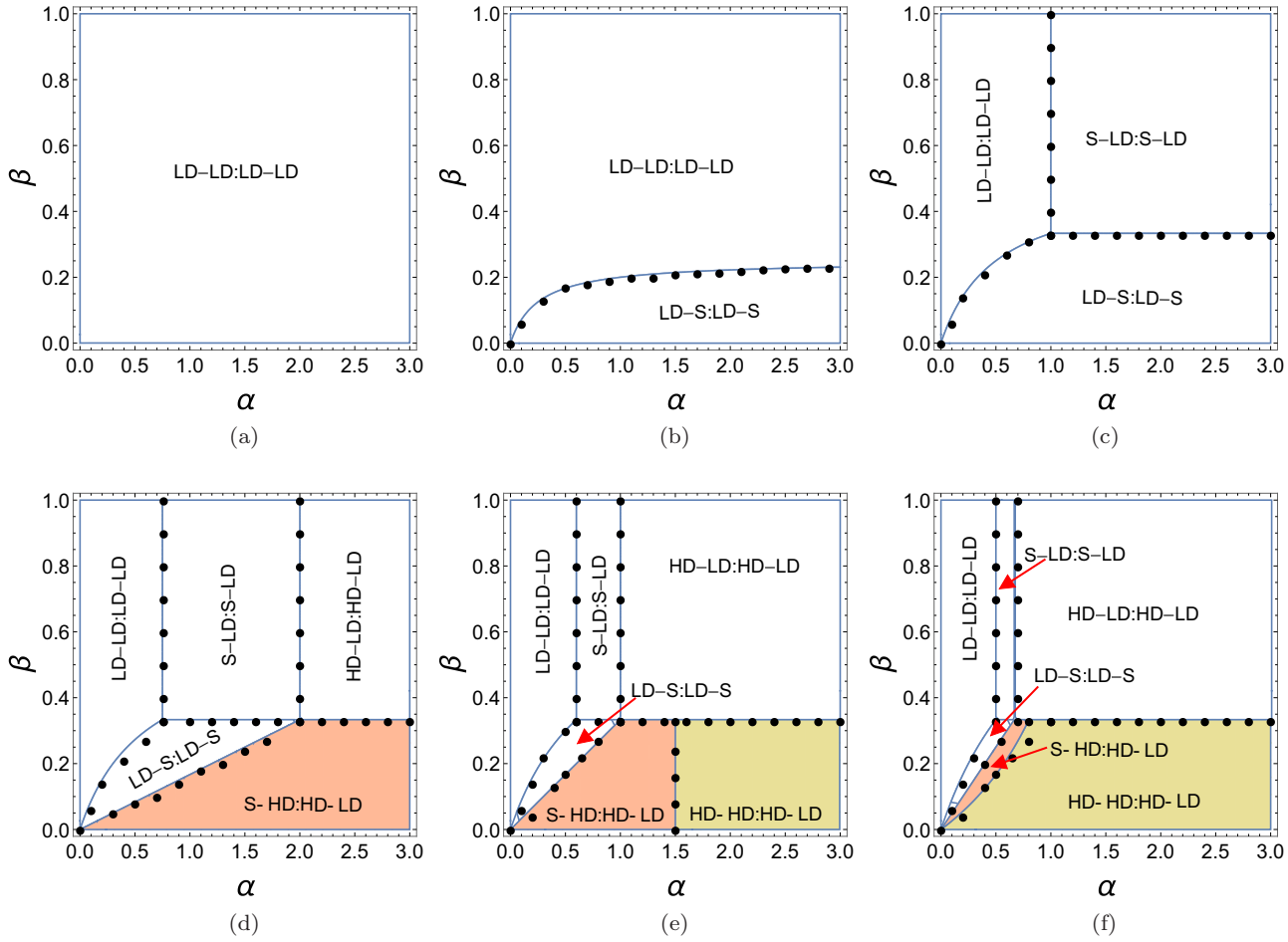

FIG. 2. Stationary phase diagrams for increasing parameter $\mu = N_{\text{tot}}/N$ (a) $\mu = 0.001$, (b) $\mu = 0.5$, (c) $\mu = 1$, (d) $\mu = 1.2$, (e) $\mu = 1.5$, and (f) $\mu = 2$. In the limiting case $\mu \to \infty$, the phase diagram converges to the two intersecting lane models with infinite particles [30]. The white colored regions represent symmetric phases, whereas, the colored regions denote asymmetric phases. The black circles are the simulated results indicating the phase boundaries computed within an estimated error of less than 1%.

a bulk induced shock emerges in the left segment of each lane resulting in a new symmetric regime S-LD:S-LD as shown in Fig. 2(c). This critical value is computed from Eq. (A26) that yields $\mu_{C_1} = 2/3$ and,

$$\alpha = \frac{\mu}{3\mu - 2}, \qquad \beta \geqslant 1/3. \tag{31}$$

However, for $\mu_{C_1} < \mu \leqslant \mu_{C_2}$ no new phase appears in the phase diagram, only quantitative changes are observed.

2. $\mu > 1$ *(symmetry breaking)*

Distinctively, beyond a critical value μ_{C_2} in addition to the emergence of a new symmetric phase the system experiences rich topological changes with the occurrence of the symmetry breaking phenomenon. As soon as $\mu > \mu_{C_2}$, a new symmetric HD-LD:HD-LD phase emerges next to the S-LD:S-LD phase resulting in the shrinkage of observed symmetric until now as shown in Fig. 2(d). From Eq. (A15), we observe that this phase exists for boundary controlling parameters satisfying

$$\alpha = \frac{\mu}{3(\mu - 1)}, \qquad \beta \geqslant 1/3. \tag{32}$$

that yields the critical value of $\mu_{C_2} = 1$. In addition, due to interaction of particles at intersected site asymmetric S-HD:HD-LD phase emerges in the (α, β) plane. This is because with an increase in the number of particles, the boundary induced shock in the LD-S:LD-S phase absorbs the incoming particles and the position of shock shifts towards the left side of each lane. Furthermore, as soon the shock position reaches to the intersected site with an increase in μ, the particle at the intersected site totally blocks the flow of particles resulting in the HD-LD phase in one lane (say lane L). For the other lane (T) the boundary induced shock crosses the intersected site and shifts to the left segment. The phase boundary for which is obtained from Eq. (B10) that leads to

$$\alpha = \frac{\beta\mu}{\mu - 1}, \qquad \beta \leqslant 1/3. \tag{33}$$

On further increasing μ after a crucial value $\mu_{C_3} = 1$ obtained from (33) and μ_{C_2} an additional asymmetric phase HD-HD:HD-LD emerges in the phase schema [as prescribed in Fig. 2(e)] for

$$\alpha = \frac{2\beta\mu}{2(\mu + \beta) - 3}, \qquad \beta \leqslant 1/3, \tag{34}$$

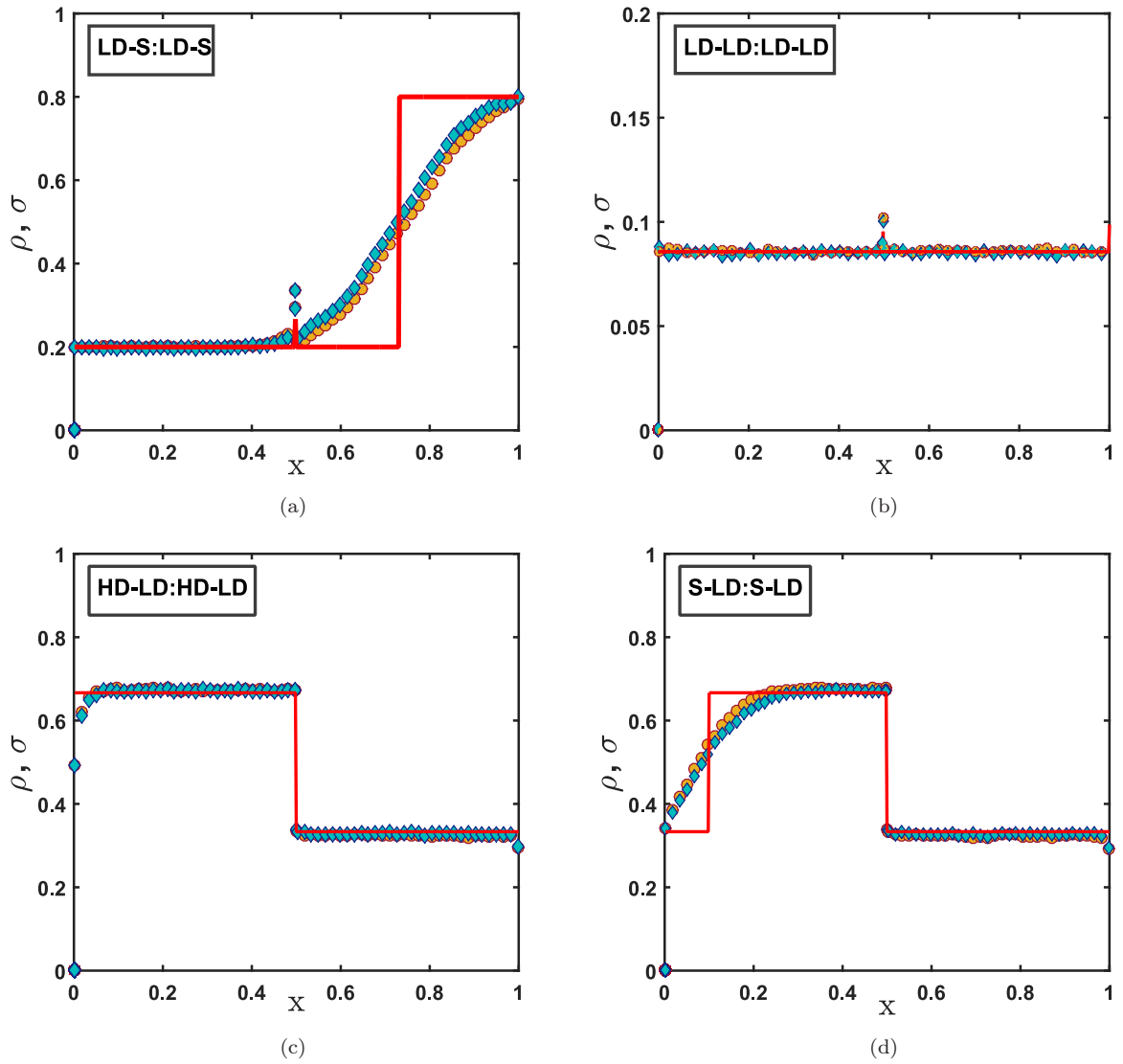

FIG. 3. Density profiles attributed to symmetric phases for (a) $\alpha = 0.5$, $\beta = 0.2$, (b) $\alpha = 0.1$, $\beta = 0.8$, (c) $\alpha = 2.5$, $\beta = 0.8$, (d) $\alpha = 1.5$, $\beta = 0.8$ with fixed parameter $\mu = 1.2$. Solid lines represent theoretical results, whereas markers denote the simulated results.

and crucial value is obtained as $\mu_{C_4} = 1.1$. This happens because as soon as a particle enters the lane for the entry rate satisfying Eq. (B22), it is quickly assimilated by the segment that exhibits shock in the S-HD:HD-LD phase. Beyond this crucial value μ_{C_3}, we observe only quantitative alterations in the phase diagram as presented in Fig. 2(f) for $\mu = 2$. Even for a finite value of μ the phase diagram of the proposed model converges to that of two intersecting the TASEP models in Ref. [30]. However, in the limiting case $\mu \to \infty$, it is clearly evident from Eqs. (A26), (A33), and (B10) that the boundary and bulk induced shock disappear, and we retrieve the phase diagram for two intersecting lanes with an infinite number of particles.

B. Density profiles and phase transitions

The density profiles attributed to symmetric as well as asymmetric stationary phases are presented in Figs. 3 and 4, respectively. We observe that all the density profiles agree well with MCs except for the case of the shock profile where a small mismatch is seen near the discontinuity as in Figs. 3(a) and 3(d). This discrepancy is primarily due to dominating the finite size effect on the simulation outcomes. To rigorously visualize this dependency we present Fig. 5 for sufficiently large system sizes thereby substantiating the theoretical observations in the thermodynamic limit. Due to the intersection of lanes, the density profile of LD-S:LD-S, LD-LD:LD-LD, HD-HD: HD-LD, and S-HD:HD-LD phases admits a kink at the intersected site as clearly visible in Figs. 3(a), 3(b), 4(a), and 4(c), respectively.

To further inspect a deeper insight in the phenomenon of SSB, we probe particle density histograms $P(\rho_1, \rho_2)$ and $P(\sigma_1, \sigma_2)$, where ρ_j and σ_j are instantaneous particle densities on segment j ($j = 1, 2$). For $\alpha = 2.5$ and $\beta = 0.8$, we present a typical density histogram for asymmetric phases S-HD:HD-LD and HD-HD:HD-LD with $\mu = 1.2$ and $\mu =$

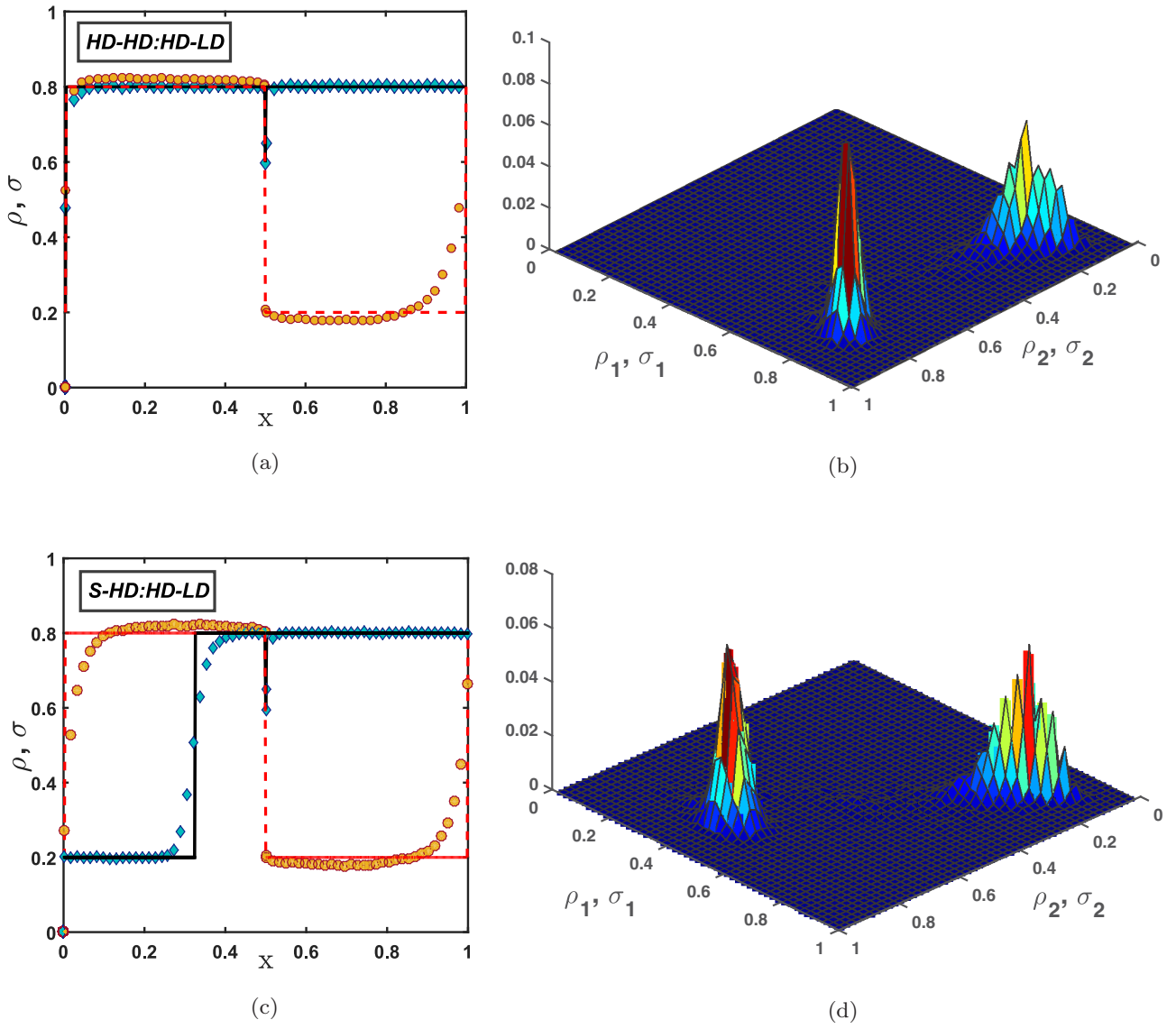

FIG. 4. (Left) Density profiles attributed to asymmetric phases for $\alpha = 2.5,\ \beta = 0.2$ in (a) and (b) and (c) and (d) with parameters $\mu = 1.5$ and $\mu = 1.2$, respectively. Such parameters are chosen to show how for a particular value of $\alpha,\ \beta$, considering different values of μ, two different asymmetric phases exist. (Left) Blue diamonds (black solid lines) and yellow circles (red dashed lines) represent simulated (corresponding theoretical) densities in lanes L and T, respectively. (Right) Particle-density histograms (b) and (d) corresponding to (a) and (c), respectively are plotted to probe the phenomenon of symmetry breaking through MCs.

1.5, respectively. One can clearly see in Fig. 4(b), the peaks in distributions are achieved for $\rho_1 = \rho_2 > 1/2$ and $\sigma_1 > 1/2,\ \sigma_2 < 1/2$ that corresponds to the HD-HD:HD-LD phase. Whereas, Fig. 4(d) demonstrates that the peak occurs for $0 < \rho_1 < 1,\ \rho_2 > 1/2$ and $\sigma_1 > 1/2,\ \sigma_2 < 1/2$ portraying the S-HD:HD-LD phase. In both cases, we observe a double peak with two off-diagonal maxima that validates the existence of asymmetric phases.

In order to visualize phase transitions with respect to μ we chose particular values of α, β and plot Fig. 6. For chosen parameters $\alpha = 2.5$ and $\beta = 0.8$, in Fig. 6(a) we portray transitions within symmetric phases LD-LD:LD-LD $\longrightarrow$ S-LD: S-LD $\longrightarrow$ HD-LD:HD-LD. When $\mu = 0.5$ the particles exhibit symmetric the LD-LD:LD-LD phase with a kink in the density profile at the intersected site. With an increase in $\mu = 1.2$, the density at the intersected site increases as also evident from Eq. (A2), that indicates the existence of the symmetric S-LD:S-LD phase. Further increasing $\mu = 1.5$, the bulk induced shock transforms into HD regime and leads to the occurrence of the symmetric HD-LD:HD-LD phase. Similarly, Fig. 6(b) illustrates the phase transitions from symmetric to asymmetric phases LD-S:LD-S $\longrightarrow$ S-HD:HD-LD $\longrightarrow$ HD-HD:HD-LD for $\alpha = 2$ and $\beta = 0.2$. When $\mu = 1$ particles manifest boundary induced shock in the right segment of both lanes displaying the symmetric LD-S:LD-S phase. Increasing $\mu = 1.2$, due to availability of an ample number of particles this shock stabilizes and transforms into asymmetric the S-HD:HD-LD phase which further converges to the asymmetric HD-HD:HD-LD phase for $\mu = 1.5$.

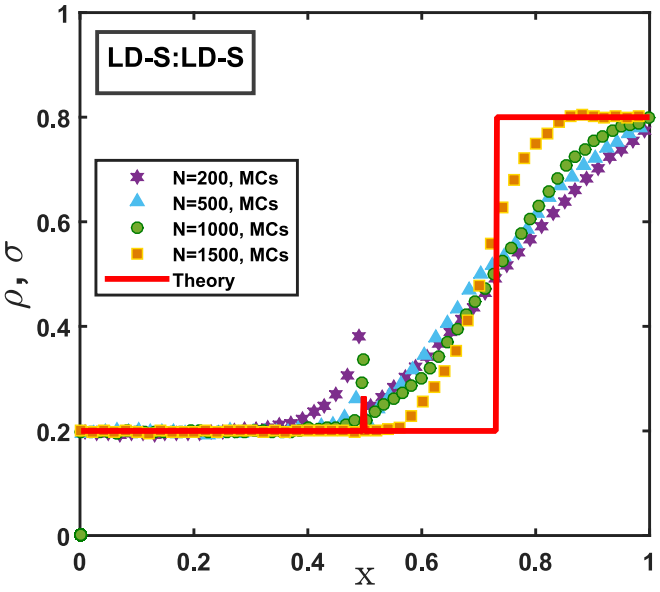

FIG. 5. Finite size effect on shock profile in the symmetric LD-S:LD-S phase for $\alpha = 0.5$, $\beta = 0.2$, and $\mu = 1.2$. Since, for symmetric phase density profiles are the same for both lanes, we plot for only one lane (say L). The colored markers denote the simulated results for various system sizes, and the red solid line signifies the theoretical mean-field results.

To summarize, there exist a maximum of six stationary phases in the overall system including four symmetric and two asymmetric phases. The complexity of the phase diagram shows nonmonotonic behavior with increasing values of μ. Initially, there exists only one phase whereas in the midrange dynamics becomes complex, and six phases are observed. Besides, the intuitive observations of the effect of finite resources, the appearance and disappearance of phases is examined from theoretically computed phase boundaries. In the limiting case $\mu \to \infty$, we have explained in Sec. IV, how effective intrinsic rate α^* approaches α in each phase. Consequently, the topological structure of phase schema is modified, and the number of phases drastically reduces from six to three [30].

C. Shock dynamics

In the above sections, we have seen that due to the finite number of particles in the system, two types of localized shock emerges in the dynamical regimes. It has been observed that a bulk induced shock exists in the symmetric S-LD:S-LD phase. Whereas a boundary induced shock persists in a symmetric LD-S:LD-S as well as an asymmetric S-HD:HD-LD phase. The shock emerging in the right segment of any lane is boundary induced, whereas that appearing in left segment might be boundary or bulk induced. Here, to discuss the phase transitions arising due to propagation of shock on the $(\alpha - \beta)$ plane we fixed a parameter and vary boundary controlling parameters (α, β).

1. Boundary induced shock

The boundary induced shock in the symmetric LD-S:LD-S phase appears in the right segment of both lanes for which the position of shock is determined by Eq. (A33) when $\beta < 1/3$. For $\beta = 0.2$, we plot Fig. 7(a) where one can note that as α increases shock shifts toward the left side of the right segment. This means, if more numbers of particles are allowed to enter the lattice for a significant choice of μ, the right segment incorporates these particles tending towards a high dense region. As soon as this wall reaches the intersected site with respect to α, interactions with other lanes are forced to exhibit the low density of particles. Thus, next to this phase with increasing α, a asymmetric phase S-HD:HD-LD appears in the steady-state phase diagram. For this phase, the position of boundary induced shock lies within the range [0,1/2] and can be computed using Eq. (B10). With an increase in α, the particles are absorbed by the segment specifying S phase. As a consequence, shock moves toward the left of the lane as

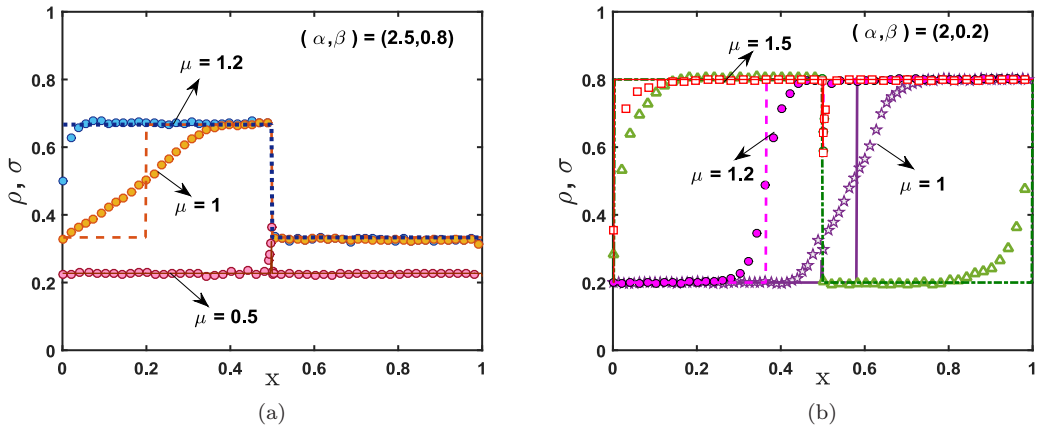

(a) (b)

FIG. 6. Phase transitions with respect to μ for fixed boundary controlling parameters (a) $\alpha = 2.5$, $\beta = 0.8$ that presents transitions within symmetric phases LD-LD: LD-LD $\longrightarrow$ S-LD: S-LD $\longrightarrow$ HD-LD: HD-LD. (b) $\alpha = 2$, $\beta = 0.2$ illustrates phase transitions from symmetric to asymmetric phases LD-S: LD-S $\longrightarrow$ S-HD: HD-LD $\longrightarrow$ HD-HD: HD-LD. Since, for the symmetric phase density the profiles are the same for both lanes, we plot for only one lane (say L). The solid and dashed lines represent theoretical results, whereas markers with similar color schemes denote the corresponding simulated outcomes.

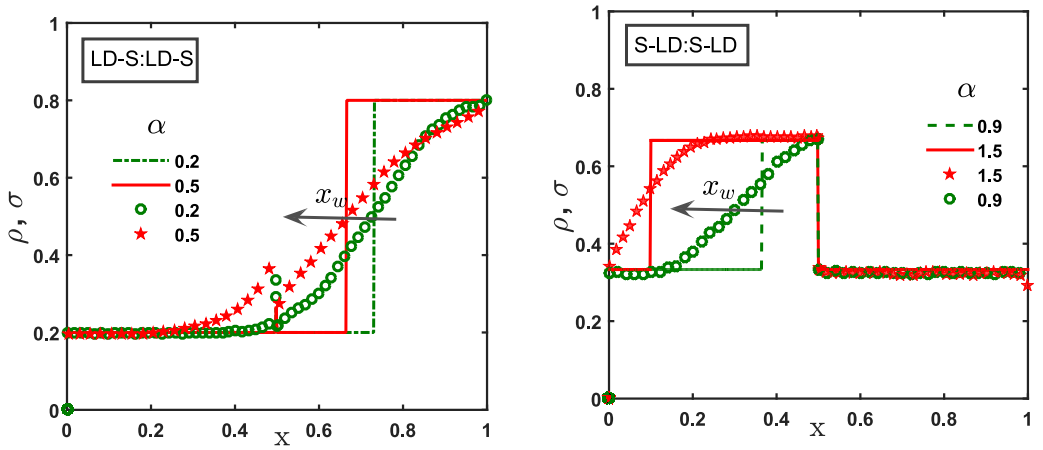

FIG. 7. Symmetric phases: Movement of shock with increasing values of α for a chosen $\mu = 1.2$ in (a) the LD-S:LD-S phase and (b) S-LD:S-LD phase for $\beta = 0.2$ and 0.8, respectively. As already discussed, the symmetric phase satisfies Eqs. (25) and (26). Therefore, without any loss of generality, we plot the density profile of particles of only one lane (say L). The same results are pertinent for the other lane T. The red solid and green dashed lines represent the theoretically computed results. Whereas, markers of similar color, i.e., red stars and green circles denote the corresponding simulated results.

shown in Fig. 8 for $\beta = 0.2$ and beyond a critical value of α, the left lane exhibits HD indicating the appearance of the asymmetric HD-HD:HD-LD phase.

2. Bulk induced shock

For $\beta > 1/3$, a bulk induced shock in the symmetric S-LD:S-LD phase appears in the phase schema. In this phase the particles in left segment of both the lanes portray a discontinuity. The explicit expression for the location of this wall is computed in Eq. (A26) that suggests for a fixed β, with an increase in α as more number of particles are permitted to enter, the shock in both lanes sweeps to the left of the lane. This can be easily noted from Fig. 7(b) where we can clearly see that as α increases for $\beta = 0.8$, the HD part of S increases and after a crucial value of α given in Eq. (32) shock vanishes. As a result, left segments of both lanes attain the HD phase leading to the occurrence of the symmetric HD-LD:HD-LD phase.

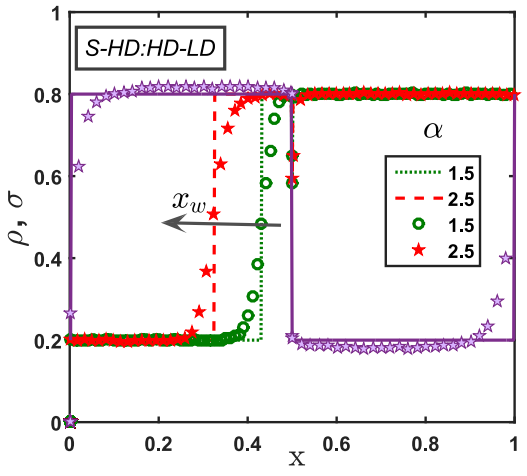

FIG. 8. Asymmetric phase: Movement of shock with increasing values of α for $\mu = 1.2$ and $\beta = 0.2$ in the S-HD:HD-LD phase. One lane portrays the HD-LD phase for chosen parameters marked with purple stars and a solid line. However, the other lane manifests the S-HD phase for which the shock position varies with α. As α increases the domain wall sweeps to the left of the lane. The red dashed and green dotted lines represent the theoretically computed results, and the same colored markers (red stars and green circles) denote the corresponding simulated results.

VI. SUMMARY AND CONCLUSION

In this paper, we have studied a specific variant of the network TASEP model with two intersecting lanes, a class of minimal models for the transportation phenomenon. The two extreme ends of each lane are connected to a reservoir having a finite number of particles. The intersection of lanes introduces an inhomogeneity in the system that is suitably dealt by considering effective entry and exit rates. Even though the particles interact at the intersected site, the mean-field approximation works well to theoretically investigate various crucial steady-state properties of the system, such as density profiles, phase transitions, and phase boundaries. The theoretical predictions are validated through extensive Monte Carlo simulations.

We extensively probe the effect of finite resources on the phenomenon of spontaneous symmetry breaking since the same persists for an infinite number of particles. With an increase in the number of particles, crucial qualitative, and quantitative changes in the topology of the phase diagram are observed. The symmetry of the phase schema is preserved until the total number of particles does not exceed the total number of sites. However, as soon as more numbers of particles are available than the number of sites, the symmetry of the phase diagram is disrupted. The interaction of particles at the intersected site is responsible for the symmetry breaking phenomenon. There exist maximum six possible stationary regimes in the system, including four symmetric

and two asymmetric phases. The exact number and location of phases depend on the number of particles in the system. The existence of asymmetric phases is explored by delineating density histograms using computer simulations. In addition, a symmetric phase exhibits a bulk and boundary induced shock in each lane. Whereas, an asymmetric phase manifests a boundary induced shock in one of the lanes due to interactions of particles at the intersected site. The density in the shock profile is estimated by employing the domain-wall approach. We explicitly calculate the phase boundaries to determine dynamic regimes and the location of different phases. Also, by monitoring the movement of shock, we describe the phase transitions as more particles are allowed to enter.

In the future, our results can serve as a base model for understanding the typical extensions by considering several generalizations. The proposed paper can be extended to analyze more complex dynamics in the network of intersecting lanes when interlane switching of particles is allowed in the bulk as well as whereas jumping from the intersected site. Also, various processes can be incorporated, such as the interplay with nonconserving dynamics, extended particle size, particle-particle interactions, etc.

ACKNOWLEDGMENT

A.K.G. acknowledges support from DST-SERB, Government Of India (Grant No. CRG/2019/004669).

APPENDIX A: SYMMETRIC PHASES

In the proposed model there are four possible symmetric phases for which we theoretically calculate phase boundaries, position of shock, and particle density in each segment. Therefore, depending on the phase we explicitly compute the expressions of effective rates α^*, $\alpha_{\rm eff}$, and $\beta_{\rm eff}$ by utilizing the theoretical framework discussed in Sec. IV A. This helps to determine the bulk density of each segment ρ_1^b, ρ_2^b, density at intersected site ρ^k and at boundaries ρ_1^{k-1} and ρ_2^{k+1}. The detailed theoretical calculations in each phase are elaborated in the following discussion.

1. LD-LD:LD-LD phase

In this phase, we assume both segments of lane L exhibit the low-density phase. Each homogeneous segment is entry dominated for which the conditions of existence are given by

$$\alpha^* < \min\{\beta_{\rm eff}, 1/2\}, \qquad \alpha_{\rm eff} < \min\{\beta, 1/2\}. \tag{A1}$$

The density of particles in the bulk of each segment is given by

$$\rho^1 = \rho_1^b = \alpha^* \quad \text{and} \quad \rho_2^{k+1} = \rho_2^b = \alpha_{\rm eff}. \tag{A2}$$

Since, the current is equal for both segments Eq. (7) results in

$$\alpha^* = \alpha_{\rm eff}. \tag{A3}$$

Solving Eq. (27), we have

$$\alpha^* = \alpha - \frac{2\alpha}{\mu}\int_0^1 \alpha^* dx, \tag{A4}$$

that leads to

$$\alpha^* = \frac{\alpha\mu}{\mu + 2\alpha}. \tag{A5}$$

The density of particles arriving from lane L at the intersected site is given by Eq. (16) $\rho^k = \alpha^*$. The effective exit rate with which a particle leaves from the left segment given in Eq. (13) reduces to

$$\beta_{\rm eff} = 1 - 2\alpha^*. \tag{A6}$$

In addition, the stationary current argument at site $k-1$ implies that the bulk current in the right segment is equal to the current entering into it that yields

$$\rho_1^{k-1} = \frac{\alpha^*(1-\alpha^*)}{1-2\alpha^*}. \tag{A7}$$

The conditions of existence for this phase, thus, reduce to

$$\alpha^* < \min\{\beta, 1/3\}. \tag{A8}$$

For the case when $\mu \to \infty$, the expression for the effective intrinsic rate in Eq. (A5) reduces to $\alpha^* = \alpha$. As a result, we retrieve the phase boundaries for the model with an infinite number of particles given by $\alpha < \min\{\beta, 1/3\}$.

2. HD-LD:HD-LD phase

We assume in this phase for each lane, the left segment to exhibit the high-density phase and the right segment in the low-density phase. Correspondingly, the homogeneous left segment is exit dominated, whereas, the right segment is entry dominated. This phase is determined by

$$\beta_{\rm eff} < \min\{\alpha^*, 1/2\}, \qquad \alpha_{\rm eff} < \min\{\beta, 1/2\}. \tag{A9}$$

The density of particles in the bulk of each segment is given by

$$\rho_1^b = \rho_1^{k-1} = 1 - \beta_{\rm eff} \quad \text{and} \quad \rho_2^b = \rho_2^{k+1} = \alpha_{\rm eff}. \tag{A10}$$

The condition of the constant current in Eq. (7) leads to

$$\beta_{\rm eff} = \alpha_{\rm eff}. \tag{A11}$$

Clearly, Eq. (16) provides the density of particles at site k as $\rho^k = \beta_{\rm eff}$. Now, plugging these values in Eq. (13) we obtain

$$\beta_{\rm eff} = 1 - 2\beta_{\rm eff}, \tag{A12}$$

implying

$$\beta_{\rm eff} = \frac{1}{3}. \tag{A13}$$

Furthermore, the effective intrinsic rate given in Eq. (27) is obtained as follows:

$$\alpha^* = \alpha - \frac{2\alpha}{\mu}\left(\int_0^{1/2}(1-\beta_{\rm eff})dx + \int_{1/2}^1 \alpha_{\rm eff}\right), \tag{A14}$$

that yields

$$\alpha^* = \alpha\left(\frac{\mu - 1}{\mu}\right). \tag{A15}$$

From the above equation we conclude that this phase exists only when $\mu > 1$. The conditions of the existence reduce to

$$1/3 < \min\{\alpha^*, \beta\}. \tag{A16}$$

In the limiting case as $\mu \to \infty$, the effective intrinsic rate in Eq. (A15) reduces to α. Correspondingly, the conditions that favor the existence of this phase reduces to $1/3 < \min\{\alpha, \beta\}$ for the model with an infinite number of particles [30].

3. S-LD:S-LD phase

For this phase, the particles in L_1 exhibit the shock phase, i.e., a part of the segment is in the LD phase and the rest is in the HD phase. Whereas, the right segment shows the low-density phase. The existence of this phase is determined by the following conditions:

$$\alpha^* = \beta_{\text{eff}}, \qquad \beta_{\text{eff}} < 1/2, \qquad \alpha_{\text{eff}} < \min\{\beta, 1/2\}. \quad \text{(A17)}$$

For this phase, in the left segment sites 1 and $k-1$ are entry and exit dominated, respectively. The density in L_1 is written as

$$\rho^1 = \alpha^*, \quad \text{(A18)}$$

$$\rho_1^{k-1} = 1 - \beta_{\text{eff}}, \quad \text{(A19)}$$

$$\int_0^{1/2} \rho_1^b dx = \int_0^{x_w} \alpha^* dx + \int_{x_w}^{1/2} (1 - \beta_{\text{eff}}) dx. \quad \text{(A20)}$$

Similarly, the density in L_2 is given by

$$\rho_2^b = \rho_2^{k+1} = \alpha_{\text{eff}}. \quad \text{(A21)}$$

Also, the current is constant in both segments as given in Eq. (7) that leads to

$$\alpha^* = \beta_{\text{eff}} = \alpha_{\text{eff}}. \quad \text{(A22)}$$

From Eq. (13) we obtain the effective exit rate of particles from the left segment as

$$\beta_{\text{eff}} = \frac{1}{3}. \quad \text{(A23)}$$

Hence, Eq. (27) yields

$$\alpha^* = \alpha - \frac{2\alpha}{\mu}\left(\int_0^{x_w} \alpha^* dx + \int_{x_w}^{1/2} (1 - \beta_{\text{eff}}) dx + \int_{1/2}^{1} \alpha^* dx\right), \quad \text{(A24)}$$

that reduces to

$$\alpha^* = \alpha\left(\frac{3(\mu - 1) + 2x_w - 1}{3\mu}\right). \quad \text{(A25)}$$

Since, $\alpha^* = \frac{1}{3}$ from Eq. (A22), the shock position is given by

$$x_w = \frac{3}{2}\left(\frac{\mu}{3\alpha} - \mu + 1\right). \quad \text{(A26)}$$

As the shock position is bounded between $0 < x_w < 1/2$ that provides one of the condition for the existence of this phase. This x_w depends on the parameters μ and α. For a fixed value of μ, as α increases shock travels to the left of the lattice on the left segments of lane L. Hence, this phase exists when

$$0 < x_w < 1/2, \qquad \beta \geqslant 1/3. \quad \text{(A27)}$$

For a system with an infinite number of particles $\mu \to \infty$, we can clearly see that $x_w \to \infty$ as a result this phase ceases to exist and converges to the HD-LD:HD-LD phase [30].

4. LD-S:LD-S phase

In each lane, the density of particles in the left segment is in the low-density phase, whereas in the right segment particles are in the shock phase. The conditions that support the existence of this phase are as follows:

$$\alpha^* < \min\{\beta_{\text{eff}}, 1/2\}, \qquad \alpha_{\text{eff}} = \beta, \qquad \beta < 1/2. \quad \text{(A28)}$$

Since, the right segment is entry dominated, we can write the density at site $k+1$, $\rho_2^{k+1} = \alpha_{\text{eff}}$. By the current constancy condition from Eq. (7), the rates are given by

$$\alpha^* = \alpha_{\text{eff}} = \beta. \quad \text{(A29)}$$

The density of particles in the left and right segments is given by

$$\rho_1^b = \rho^1 = \alpha^*, \qquad \rho_2^{k+1} = \alpha_{\text{eff}}, \quad \text{(A30)}$$

$$\int_{1/2}^{1} \rho_2^b dx = \int_{1/2}^{x_w} \alpha_{\text{eff}} dx + \int_{x_w}^{1} (1 - \beta) dx, \quad \text{(A31)}$$

respectively. As a result, solving Eq. (27) provides the effective intrinsic rate given by

$$\beta = \alpha - \frac{2\alpha}{\mu}\left(\int_0^{1/2} \beta\, dx - \int_{1/2}^{x_w} \beta\, dx - \int_{x_w}^{1} (1 - \beta) dx\right) \quad \text{(A32)}$$

that implies

$$x_w = \frac{\beta\mu - \alpha(\mu + 2\beta - 2)}{2\alpha(1 - 2\beta)}. \quad \text{(A33)}$$

For this phase to exist the shock travels within the range of $1/2 < x_w < 1$. Also, from Eq. (13) the density at the kth site is $\rho^k = \alpha_{\text{eff}} = \beta$. Hence, the effective exit rate is given as

$$\beta_{\text{eff}} = 1 - 2\beta. \quad \text{(A34)}$$

In addition, the stationary current argument at site $k-1$ implies that the bulk current in the bright segment is equal to the current entering into it that yields

$$\rho_1^{k-1} = \frac{\alpha^*(1 - \alpha^*)}{1 - 2\beta}. \quad \text{(A35)}$$

The conditions of this phase to exist are as follows:

$$1/2 < x_w < 1, \qquad \beta \leqslant 1/3. \quad \text{(A36)}$$

For $\mu \to \infty$, the computed expression for the position of shock converges to ∞. This shows that this symmetric phase vanishes when there are an infinite number of particles and tends to the LD-LD:LD-LD phase [30].

APPENDIX B: ASYMMETRIC PHASES

Based on the theoretical framework discussed in Sec. IV B, we aim to theoretically obtain the expressions of phase boundaries, shock position, and density of particles in possible asymmetric phases. The detailed calculations are discussed below in each phase to compute the expressions of effective rates that determine the stationary properties of the system.

1. S-HD:HD-LD phase

We presume particles in the left segment of lane L to exhibit the shock phase and the right segment to manifest

TABLE IV. Conditions for the existence of the asymmetric S-HD:HD-LD phase.

	L	T
Left segment	$\alpha^* = \beta_{\text{eff}},\ \beta_{\text{eff}} < 1/2$	$\beta_{\text{eff}} < \min\{\alpha^*, 1/2\}$
Right segment	$\beta < \min\{\alpha_{\text{eff},L}, 1/2\}$	$\alpha_{\text{eff},T} < \min\{\beta, 1/2\}$

TABLE V. Conditions for the existence of the asymmetric HD-HD:HD-LD phase.

	L	T
Left segment	$\beta_{\text{eff}} < \min\{\alpha^*, 1/2\}$	$\beta_{\text{eff}} < \min\{\alpha^*, 1/2\}$
Right segment	$\beta < \min\{\alpha_{\text{eff},L}, 1/2\}$	$\alpha_{\text{eff}} < \min\{\beta, 1/2\}$

the high-density phase. Although the particles in the left and right segments of lane T display high- and low-density phases, respectively. This phase exists when the boundary controlling parameters satisfy the following conditions described in Table IV. The density in bulk of the two segments of lane L is given by

$$\rho_1^{k-1} = 1 - \beta_{\text{eff}}, \tag{B1}$$

$$\int_0^{1/2} \rho_1^b dx = \int_0^{x_w} \alpha^* dx + \int_{x_w}^{1/2} (1 - \beta_{\text{eff}}) dx, \tag{B2}$$

$$\rho_2^b = 1 - \beta. \tag{B3}$$

Next, the density in the bulk of the left and right segments of lane T is given by

$$\sigma_1^{k-1} = \sigma_1^b = 1 - \beta_{\text{eff}}, \tag{B4}$$

$$\sigma_2^{k+1} = \sigma_2^b = \alpha_{\text{eff},T}, \tag{B5}$$

respectively. Since the current is constant in each segment of L, from Eq. (8) we have

$$\alpha^*(1 - \alpha^*) = \beta_{\text{eff}}(1 - \beta_{\text{eff}}) = \beta(1 - \beta), \tag{B6}$$

and similarly for lane T, we can write

$$\beta_{\text{eff}}(1 - \beta_{\text{eff}}) = \alpha_{\text{eff},T}(1 - \alpha_{\text{eff},T}). \tag{B7}$$

This yields

$$\alpha^* = \alpha_{\text{eff},T} = \beta, \tag{B8}$$

and these values are further substituted in Eq. (22) to evaluate the shock position in L_1,

$$\beta = \alpha - \frac{\alpha}{\mu}\left(\int_0^{x_w} \beta\, dx + \int_{x_w}^{1/2} (1 - \beta) dx + \int_0^{1} (1 - \beta) dx + \int_{1/2}^{1} \beta\, dx \right). \tag{B9}$$

The shock position x_w is obtained as

$$x_w = \frac{2\mu(\beta - \alpha) + \alpha(3 - 2\beta)}{2\alpha(1 - 2\beta)}, \tag{B10}$$

that lies in [0,1/2]. From Eq. (13), plugging $\sigma^k = \alpha_{\text{eff},T} = \beta$ we have

$$\beta_{\text{eff}} = 1 - \rho^k - \beta, \tag{B11}$$

that provides the density of particles arriving from lane L at the intersected site, given by

$$\rho^k = 1 - 2\beta. \tag{B12}$$

This gives the effective entry rate of particles in L_2, $\alpha_{\text{eff},L} = 1 - 2\beta$. Hence, this phase exists for

$$0 < x_w < 1/2, \qquad \beta \leqslant 1/3. \tag{B13}$$

Under these conditions, one can easily obtain that this phase exists only when $\mu > 1$. However, for $\mu \to \infty$, $x_w \to \infty$ that implies this phase vanishes in the limiting case of an infinite number of particles and converges to the HD-HD:HD-LD phase [30].

2. HD-HD:HD-LD phase

Without any loss of generality in this phase, we assume both segments of lane L exhibit high density, whereas, the left and right segments of T display high and low densities, respectively. This phase exists when boundary controlling parameters satisfy the conditions presented in Table V.

The density in each segment is given by

$$\rho_1^b = \rho_1^{k-1} = 1 - \beta_{\text{eff}} \quad \text{and} \quad \rho_2^b = 1 - \beta, \tag{B14}$$

$$\sigma_1^b = \sigma_1^{k-1} = 1 - \beta_{\text{eff}} \quad \text{and} \quad \sigma_2^b = \sigma_2^{k+1} = \alpha_{\text{eff},T}. \tag{B15}$$

Since the current is constant in each lane given in Eq. (7) yields

$$\beta_{\text{eff}} = \beta, \tag{B16}$$

$$\beta_{\text{eff}} = \alpha_{\text{eff},T}, \tag{B17}$$

that implies

$$\alpha_{\text{eff},T} = \beta = \sigma^k \tag{B18}$$

giving density of particles from lane T at the intersected site. The effective intrinsic rate is calculated utilizing Eq. (22) that leads to

$$\alpha^* = \alpha\left(\frac{2\mu + 2\beta - 3}{2\mu}\right). \tag{B19}$$

From Eq. (13) we have

$$\beta_{\text{eff}} = 1 - \rho^k - \beta, \tag{B20}$$

that gives the particle density of particles from lane L as

$$\rho^k = 1 - 2\beta. \tag{B21}$$

As a result the existence of conditions for this phase reduce to

$$\frac{\alpha(3 - 2\mu)}{2(\alpha - \mu)} < \beta, \qquad \beta \leqslant 1/3. \tag{B22}$$

Combing these conditions, we can easily conclude that this phase exists when $\mu > 1.1$. Here, in the limiting case $\mu \to \infty$, the conditions of existence reduce to $\alpha < \min\{\beta, 1/3\}$, that for the model with two intersecting lanes and an infinite number of particles [30].

However, it is notable that not all combinations for asymmetric phases exist in the proposed model. For instance, suppose lane L exhibits high density in both segments and lane T displays low density in both segments. The conditions of existence for this HD:HD-LD:LD phase are given by

$$\text{Lane } L, \qquad \beta < \{\alpha^*, 1/2\}, \tag{B23}$$

$$\text{Lane } T, \qquad \alpha^* < \{\beta, 1/2\}, \tag{B24}$$

which contradict each other. Similarly, other asymmetric phases cease to exist because either the conditions disagree or no values of (α, β) satisfy these conditions.

[1] G. Schutz, *Phase Transitions and Critical Phenomena* (Academic Press, 2000), Chap. 1.
[2] F. Spitzer, *Random Walks, Brownian Motion, and Interacting Particle Systems* (Springer, Birkhäuser, Boston, MA, 1991), pp. 66–110.
[3] H. Spohn, *Large Scale Dynamics of Interacting Particles* (Springer Science, Berlin, 2012).
[4] B. Derrida, E. Domany, and D. Mukamel, J. Stat. Phys. **69**, 667 (1992).
[5] A. Parmeggiani, T. Franosch, and E. Frey, Phys. Rev. Lett. **90**, 086601 (2003).
[6] C. T. MacDonald, J. H. Gibbs, and A. C. Pipkin, Biopolymers **6**, 1 (1968).
[7] C. T. MacDonald and J. H. Gibbs, Biopolymers **7**, 707 (1969).
[8] K. Mallick, J. Stat. Mech.: Theory Exp. (2011) P01024.
[9] A. Schadschneider, Physica A **285**, 101 (2000).
[10] D. Helbing, Rev. Mod. Phys. **73**, 1067 (2001).
[11] T. Chou, K. Mallick, and R. Zia, Rep. Prog. Phys. **74**, 116601 (2011).
[12] I. Neri, N. Kern, and A. Parmeggiani, Phys. Rev. Lett. **107**, 068702 (2011).
[13] B. Embley, A. Parmeggiani, and N. Kern, Phys. Rev. E **80**, 041128 (2009).
[14] M. Basu and P. Mohanty, J. Stat. Mech.: Theory Exp. (2010) P10014.
[15] I. Neri, N. Kern, and A. Parmeggiani, New J. Phys. **15**, 085005 (2013).
[16] M. E. Fouladvand, Z. Sadjadi, and M. R. Shaebani, J. Phys. A **37**, 561 (2004).
[17] T. Thunig and K. Nagel, Procedia Comput. Sci. **83**, 946 (2016).
[18] L. Crociani, G. Lämmel, and G. Vizzari, in *International Conference on Cellular Automata* (Springer, Cham, 2016), pp. 415–423.
[19] J. Cividini, H. Hilhorst, and C. Appert-Rolland, J. Phys. A: Math. Theor. **46**, 345002 (2013).
[20] H. Hilhorst and C. Appert-Rolland, J. Stat. Mech.: Theory Exp. (2012) P06009.
[21] A. Raguin, N. Kern, and A. Parmeggiani, J. Theor. Biol. **505**, 110370 (2020).
[22] Y. Ishibashi and M. Fukui, J. Phys. Soc. Jpn. **65**, 2793 (1996).
[23] Y. Ishibashi and M. Fukui, J. Phys. Soc. Jpn. **70**, 3747 (2001).
[24] Y. Ishibashi and M. Fukui, J. Phys. Soc. Jpn. **70**, 2793 (2001).
[25] H.-F. Du, Y.-M. Yuan, M.-B. Hu, R. Wang, R. Jiang, and Q.-S. Wu, J. Stat. Mech.: Theory Exp. (2010) P03014.
[26] S. Bittihn and A. Schadschneider, Phys. Rev. E **94**, 062312 (2016).
[27] E. I. Pas and S. L. Principio, Transp. Res. Part B: Methodol. **31**, 265 (1997).
[28] D. Braess, A. Nagurney, and T. Wakolbinger, Transp. Sci. **39**, 446 (2005).
[29] Y.-M. Yuan, R. Jiang, R. Wang, Q.-S. Wu, and J.-Q. Zhang, J. Phys. A: Math. Theor. **41**, 035003 (2008).
[30] B. Tian, R. Jiang, M.-B. Hu, Z.-J. Ding, and B. Jia, Europhys. Lett. **128**, 40005 (2020).
[31] B. Tian, R. Jiang, M.-B. Hu, Z.-J. Ding, and B. Jia, Physica A **541**, 123542 (2020).
[32] M. R. Evans, D. P. Foster, C. Godrèche, and D. Mukamel, Phys. Rev. Lett. **74**, 208 (1995).
[33] M. Evans, D. Foster, C. Godreche, and D. Mukamel, J. Stat. Phys. **80**, 69 (1995).
[34] S. Muhuri and I. Pagonabarraga, J. Stat. Mech.: Theory Exp. (2011) P11011.
[35] V. Popkov, M. R. Evans, and D. Mukamel, J. Phys. A: Math. Theor. **41**, 432002 (2008).
[36] E. Pronina and A. B. Kolomeisky, J. Phys. A: Math. Theor. **40**, 2275 (2007).
[37] N. Sharma and A. Gupta, J. Stat. Mech.: Theory Exp. (2017) 043211.
[38] A. K. Verma, N. Sharma, and A. K. Gupta, Phys. Rev. E **97**, 022105 (2018).
[39] D. Adams, B. Schmittmann, and R. Zia, J. Stat. Mech.: Theory Exp. (2008) P06009.
[40] M. Ha and M. den Nijs, Phys. Rev. E **66**, 036118 (2002).
[41] T. L. Blasius, N. Reed, B. M. Slepchenko, and K. J. Verhey, PLoS One **8**, e76081 (2013).
[42] L. Ciandrini, I. Neri, J. C. Walter, O. Dauloudet, and A. Parmeggiani, Phys. Biol. **11**, 056006 (2014).
[43] A. K. Verma and A. K. Gupta, J. Phys. Commun. **2**, 045020 (2018).
[44] P. Greulich, L. Ciandrini, R. J. Allen, and M. C. Romano, Phys. Rev. E **85**, 011142 (2012).
[45] L. J. Cook and R. Zia, J. Stat. Mech.: Theory Exp. (2009) P02012.
[46] L. J. Cook, R. K. P. Zia, and B. Schmittmann, Phys. Rev. E **80**, 031142 (2009).
[47] B. Derrida, M. R. Evans, V. Hakim, and V. Pasquier, J. Phys. A **26**, 1493 (1993).
[48] G. Schütz and E. Domany, J. Stat. Phys. **72**, 277 (1993).
[49] R. A. Blythe and M. R. Evans, J. Phys. A: Math. Theor. **40**, R333 (2007).
[50] A. B. Kolomeisky, G. M. Schütz, E. B. Kolomeisky, and J. P. Straley, J. Phys. A **31**, 6911 (1998).
[51] E. Pronina and A. B. Kolomeisky, J. Stat. Mech.: Theory Exp. (2005) P07010.
[52] A. De masi, C. Kipnis, E. Presutti, and E. Saada, Stochast. Stochast. Rep. **27**, 151 (1989).